

TOWARDS CONSISTENT MODELING OF ATMOSPHERIC CHEMISTRY AND DYNAMICS IN EXOPLANETS: VALIDATION AND GENERALIZATION OF CHEMICAL RELAXATION METHOD

SHANG-MIN TSAI¹, DANIEL KITZMANN¹, JAMES R. LYONS², JOÃO MENDONÇA^{1,3,4}, SIMON L. GRIMM¹, KEVIN HENG¹

¹University of Bern, Center for Space and Habitability, Gesellschaftsstrasse 6, CH-3012, Bern, Switzerland. Email: shang-min.tsai@space.unibe.ch, kevin.heng@csh.unibe.ch

²Arizona State University, School of Earth & Space Exploration, Tempe, Arizona 85281 U.S.A.

³University of Copenhagen, Centre for Star and Planet Formation, Niels Bohr Institute and Natural History Museum of Denmark, Østervoldgade 5–7, 1350 Copenhagen K, Denmark

⁴Astrophysics and Atmospheric Physics, National Space Institute, Technical University of Denmark, Elektrovej, 2800, Kgs. Lyngby, Denmark

ABSTRACT

Motivated by the work of Cooper & Showman, we revisit the chemical relaxation method, which seeks to enhance the computational efficiency of chemical-kinetics calculations by replacing the chemical network with a handful of independent source/sink terms. Chemical relaxation solves the evolution of the system and can treat disequilibrium chemistry, as the source/sink terms are driven towards chemical equilibrium on a prescribed chemical timescale, but it has surprisingly never been validated. First, we generalize the treatment by forgoing the use of a single chemical timescale, instead developing a pathway analysis tool that allows us to identify the rate-limiting reaction as a function of temperature and pressure. For the interconversion between methane and carbon monoxide and between ammonia, and molecular nitrogen, we identify the key rate-limiting reactions for conditions relevant to currently characterizable exo-atmospheres (500–3000 K, 0.1 mbar to 1 kbar). Second, we extend chemical relaxation to include carbon dioxide and water. Third, we examine the role of metallicity and carbon-to-oxygen ratio in chemical relaxation. Fourth, we apply our pathway analysis tool to diagnose the differences between our chemical network and that of Moses and Venot. Finally, we validate the chemical relaxation method against full chemical kinetics calculations in one dimension. For WASP-18b-, HD 189733b- and GJ 1214-b-like atmospheres, we show that chemical relaxation is mostly accurate to within an order of magnitude, a factor of 2 and $\sim 10\%$, respectively. The level of accuracy attained allows for the chemical relaxation method to be included in three-dimensional general circulation models.

Keywords: planets and satellites: atmospheres – planets and satellites: composition – methods: numerical

1. INTRODUCTION

The study of exoplanets has evolved from detection to characterization, thanks to the advent of cutting-edge observational techniques. The spectra of exo-atmospheres provide us with valuable clues about the atmospheric chemistry and thermal structure. Diagnosing and interpreting these spectra to obtain chemical compositions is now at the forefront of exo-atmospheric research.

The simplest assumption is to build a model in chemical equilibrium, where the molecular composition for a given elemental abundance only depends on local, basic parameters (pressure and temperature) independent of the reaction pathways. However, equilibrium chemistry only holds in the hot ($T \gtrsim 2000$ K) or deep ($P \gtrsim 100$ bar) parts of the atmosphere. Processes like ultraviolet (UV) irradiation and atmospheric dynamics drive the chemical composition in the observable atmosphere away from equilibrium. These disequilibrium processes commonly dominate the observable parts of atmospheres in the Solar System.

Chemical kinetics models, which incorporate a chemical network of hundreds to thousands of reactions, are needed to study disequilibrium chemistry (e.g., [Kopparapu, Kasting & Zahnle 2012](#); [Moses et al. 2011](#); [Venot et al. 2012](#); [Grassi et al. 2014](#); [Venot et al. 2012](#); [Hu & Seager 2014](#); [Rimmer & Helling 2016](#); [Tsai et al. 2017](#)). Even with such a number of reactions, chemical networks are greatly reduced compared to Nature and restricted to measurements in specific temperature ranges. In other words, there does not exist a one-fits-all chemical network in practice. The accuracy of a network is determined by whether it includes the relevant reactions and if the input rate coefficients are reliable. Unfortunately, these chemical kinetics models are expensive to run, especially when one desires to couple chemistry to three-dimensional atmospheric motion. In one dimension, eddy diffusion is used to mimic large-scale atmospheric circulation, convection, turbulence, etc. The three-dimensional atmospheric circulation patterns of tidally-locked, highly-irradiated exoplanets are demonstrably more complicated (e.g., [Showman et al.](#)

2009; Dobbs-Dixon & Agol 2013 and see Heng & Showman 2015 for a review). In order to correctly interpret the transmission spectra of hot Jupiters, there is a need to develop three-dimensional general circulation models (GCMs) that couple the atmospheric dynamics and chemistry. Intermediate steps have already been taken in this direction by, e.g., Agúndez et al. (2012, 2014), who coupled a chemical kinetics code to a simplified model of the atmospheric dynamics (constant solid-body rotation mimicking a uniform equatorial jet). There is clearly a need to build on studies like these, but a brute-force coupling between a three-dimensional solver of the fluid equations and a chemical kinetics code with a network of hundreds to thousands of reactions is computationally challenging, even without considering radiative transfer (which is needed to include photochemistry).

Another approach is to simplify the chemical scheme. Conceptually, the interaction between atmospheric motion and chemistry is a comparison between two timescales: the dynamical versus chemical timescales. The simplest approach is to use the timescale argument, or quenching approximation. It assumes that the deep atmosphere is in chemical equilibrium, because the chemical timescale is much shorter than the dynamical timescale. There is a location within the atmosphere known as the quench point, where the timescales are equal. Above the quench point, the chemical abundances are assumed to be well-mixed and frozen to their equilibrium values at the quench point. In technical parlance, the process is referred as “transport-induced quenching”. The quenching approximation has been used to understand the over-abundance of carbon monoxide (CO) in the upper troposphere of Jupiter (Prinn & Barshay 1977). Visscher (2012) compared the chemical timescale for converting methane (CH₄) to CO to the orbital timescales of highly eccentric exoplanets to study the interaction between the evolving thermal structures and the chemistry. While the quenching approximation can be used to build the bulk of our intuition, it has been shown that it should be applied with caution to know when the abundance of a molecule is controlled by the disequilibrium abundance of another parent molecule, e.g., acetylene being controlled by methane (Tsai et al. 2017). Additionally, the quenching approximation contains the ambiguity of having to specify an appropriate length scale, which is not known from first principles (Smith 1998).

A more realistic approach is chemical relaxation. It was pioneered in the exo-atmospheres literature by Cooper & Showman (2006). Instead of simplifying the treatment of atmospheric dynamics, chemical relaxation takes the approach of replacing the chemical network with a single source/sink term that depends on the chemical timescale. Cooper & Showman (2006) coupled chemical relaxation to a simplified GCM to study quenching of CO, and suggested that most of the carbon is locked up in CO in HD 209458b due to transport. However, a shortcoming of their study is the assumption of a single rate-limiting reaction for the interconversion and

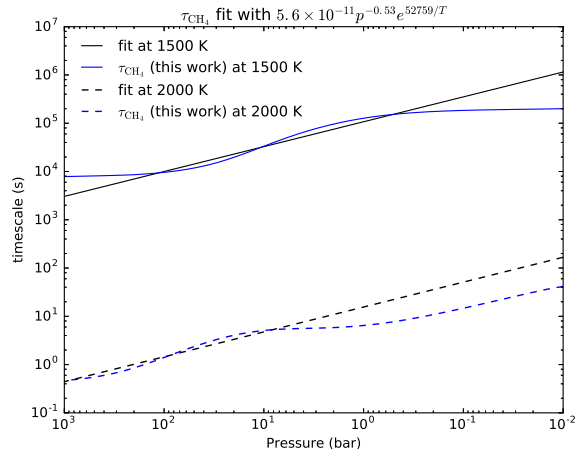


Figure 1. Chemical timescales associated with methane for 1500 K (blue solid curve) and 2000 K (blue dashed curve) computed using full chemical kinetics. Following Figure 5 of Zahnle & Marley (2014)¹, we found a fit for τ_{CH_4} in the range of $1300 \text{ K} \lesssim T \lesssim 2200 \text{ K}$ and $0 \lesssim P \lesssim 100 \text{ bar}$: $5.6 \times 10^{-11} p^{-0.53} e^{52759/(K)/T}$. We then overlaid this Arrhenius-like fit (black, solid and dashed curves) with full chemical-kinetics calculations of τ_{CH_4} , over a broader range of pressures, in for two values of the temperature (1500 and 2000 K).

probably the underestimation of the timescale of CO.

A prerequisite for implementing chemical relaxation is to be able to compute the chemical timescale over a broad range of temperatures and pressures. Initially, we had hoped to seek a universal fit for the chemical timescale across temperature, pressure and metallicity, motivated by the work of Zahnle & Marley (2014). Figure 1 shows our attempt at fitting an Arrhenius-like function to the chemical timescale for CH₄-CO conversion. We find the timescales explored in Zahnle & Marley (2014) are likely restricted to a narrow temperature-pressure range. It is apparent that such a simple approach fails to fit the timescale across the range of values of temperature and pressure needed for us to implement chemical relaxation.

Generally, the chemical timescale is a *function* that draws upon different rate-limiting reactions in different temperature and pressure regimes. A challenge with the chemical relaxation method is to find these rate-limiting reactions. In doing so, we develop a simple method to identify the dominant pathway and the associated rate-limiting step (RLS) in the chemical network for given values of the temperature, pressure, and elemental abundances. The pathway analysis can be used for comparing chemical kinetics calculations performed by different groups using different chemical networks, as it allows one to identify the key reactions that essentially control the output, and assess if key reactions are

¹ Note that τ_{CO} is not distinguished from τ_{CH_4} in Zahnle & Marley (2014): these two timescales are only equal when $[\text{CO}]/[\text{CH}_4] = 1$. We find in fact the left panel in Figure 5 of Zahnle & Marley (2014) shows τ_{CH_4} and the right panel shows τ_{CO} due to different temperatures.

missing. It is useful both on from a practical point of view and for developing physical intuition (e.g., [Turányi 1990](#)).

Ever since the work of [Cooper & Showman \(2006\)](#), only [Drummond et al. \(2018\)](#) has recently implemented the relaxation method in the Met Office Unified Model and improved it by consistently coupling to radiative transfer. However, to our knowledge, chemical relaxation has surprisingly never been validated. By “validation”, we mean that the accuracy of chemical relaxation should be demonstrated to a factor of a few, rather than to $\sim 1\%$ accuracy (or better), given the existing uncertainties in the rate coefficients and the approximate nature of the approach. In addition, transit radii are proportional to the logarithms of the chemical abundances, such a factor-of-several validation suffices for studying atmospheric chemistry in hot Jupiters. In the current study, we perform this validation step in one dimension, since it is a test of the ability of the chemical relaxation scheme to mimic the full chemical network, rather than one of the complicated three-dimensional geometry. In a future work, we will aim to couple the chemical relaxation scheme to a three-dimensional GCM, but in the current work we restrict ourselves to validating the scheme on a factor-of-several basis. Such a strategy follows the well-established hierarchical approach of constructing climate models ([Held 2005](#)). We do not consider photochemistry for the current study.

In §2, we provide the background theory on how to compute the chemical timescale. In §3, we describe our methodology for identifying the rate-limiting chemical reactions. In §4, we describe how we compute the chemical timescales. In §5, we compare our chemical network to that of Moses and Venot using our pathway analysis tool. In §6, we validate the chemical relaxation method for three model atmospheres. In §7, we summarize our findings and list opportunities for future work.

2. SIMPLIFIED EXPRESSION FOR REACTION RATE EQUATIONS

To compute the chemical timescale for use in the chemical relaxation method, we need to first derive a simplified expression for it that depends only on the local conditions of temperature and pressure. This allows us to evaluate the rate of change of the abundances efficiently.

Consider a chemical species subject to production (\mathcal{P}) and loss (\mathcal{L}) through a network of chemical reactions without any disequilibrium process (e.g., transport). The rate of change of its volume number density (n) is

$$\frac{dn}{dt} = \mathcal{P} - n\mathcal{L}. \quad (1)$$

Equation (1) is written in a way that \mathcal{P} and \mathcal{L} do not depend on n , as production only depends on other species and loss depends linearly on the number density of the reactant for a typical bimolecular reaction. Since \mathcal{P} and \mathcal{L} depend on the number densities of other species, the ensemble of equation

(1) for every species forms a system of coupled differential equations and the calculation involves inverting a large matrix (e.g., [Hu, Seager & Bains 2012](#); [Tsai et al. 2017](#)). If one wishes to implement chemical kinetics into the dynamical core of a GCM, then one needs to include a separate Euler equation for every species in the chemical network.

The relaxation method rewrites equation (1) as ([Smith 1998](#); [Cooper & Showman 2006](#))

$$\frac{dn}{dt} = -\frac{n - n_{\text{EQ}}}{\tau_{\text{chem}}}, \quad (2)$$

replacing the production and loss terms with a source/sink term that relaxes n to n_{EQ} by the chemical timescale (τ_{chem}). When the abundance is greater (less) than its equilibrium value, then it decreases (increases) and works its way towards equilibrium. The chemical timescale is effectively determined by the employed chemical network. When coupled to a GCM, whether the species in question attains chemical equilibrium depends on the competition between atmospheric dynamics and chemistry via their corresponding timescales. Chemical relaxation is analogous to the Newtonian relaxation method used as a substitute for radiative transfer (e.g., [Held & Suarez 1994](#)) or the treatment of condensation where the supersaturated gas is relaxed to the saturated vapor number density on the condensation timescale ([Hu, Seager & Bains 2012](#)).

The chemical timescale is conventionally expressed without justification as

$$\tau_{\text{chem}} = \frac{n}{|dn/dt|} = \frac{n_{\text{EQ}}}{n'_{\text{EQ}}\mathcal{L}'_{\text{EQ}}}, \quad (3)$$

where the second equality assumes that the species in question has a number density that is equal to its chemical equilibrium value. Furthermore, $n'_{\text{EQ}}\mathcal{L}'_{\text{EQ}}$ refers to the loss rate determined by the RLS involving other species but not n , denoted with primes (The ambiguity comes from using the equilibrium abundance for the numerator but not the denominator in equation(3) since dn/dt vanishes in chemical equilibrium).

We now wish to demonstrate that equation (3) may be derived from equation (1) and (2). First, consider the situation when $n \ll n_{\text{EQ}}$. This implies that the loss of the species being considered is negligible compared to production, which means $dn/dt \approx \mathcal{P}$. If we assume that all of the other species in the network are close to chemical equilibrium (as most of the intermediate species are fast-reacting radicals), then we can further write $\mathcal{P} \approx \mathcal{P}'_{\text{EQ}}$ because recall that \mathcal{P} does not depend on n . For the RLS, we can write $\mathcal{P}'_{\text{EQ}} = n'_{\text{EQ}}\mathcal{L}'_{\text{EQ}}$. By inserting this expression into equation (1) and (2), we obtain equation (3). In the opposite limit of $n \gg n_{\text{EQ}}$, the loss of the species dominates production and we have $dn/dt = -n\mathcal{L} \approx -n'_{\text{EQ}}\mathcal{L}'_{\text{EQ}}$. This again leads to equation (3) from equation (1) and (2). Since the chemical timescale expression is approximately correct for both limits, it is expected to work at order-of-magnitude accuracy at least. This

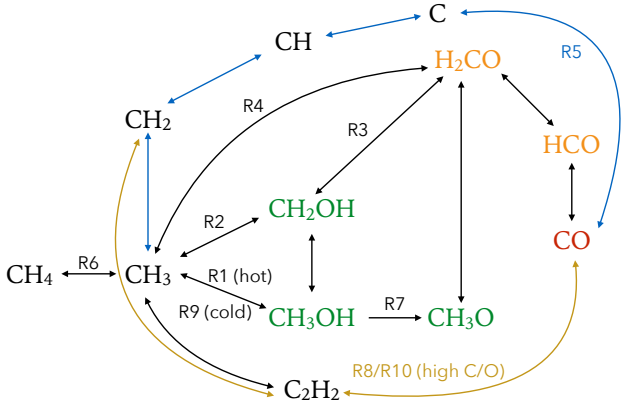


Figure 2. Visualization of the major chemical pathways between methane and carbon monoxide in hydrogen-dominated atmospheres. The triple, double and single bonds between carbon and oxygen are colored red, orange and green, respectively. The blue arrows represent the pathway at high temperatures and low pressures for $C/O < 1$. The brown arrows represent the pathway turned up for $C/O > 1$. For a description of the (R1) to (R10) reactions, see text. For their specific operating temperatures and pressures, see Tables 2 (solar abundance) and 3 ($C/O=2$).

expectation will be confirmed by full numerical calculations of chemical kinetics.

3. DETERMINING THE RATE-LIMITING REACTIONS IN THE CHEMICAL NETWORK

It is common for the chemical conversion of one species to another to not occur in one step. Rather, it takes multiple steps to surmount the energy barrier via the breaking or forming of chemical bonds. These sequence of reactions form a pathway, and the chemical timescales associated with each step in the pathway may differ by many orders of magnitude. The efficiency of a pathway is bottlenecked by its slowest reaction. Specifically, *the RLS is defined as the slowest reaction along the fastest pathway*. It informs the effective loss rate, $n'_{EQ} \mathcal{L}'_{EQ}$, in equation (3). Thus, computing the chemical timescale involves identifying the RLS. For example, Zahnle & Marley (2014) have remarked how the conversion of CO to CH₄ may be visualized as the reduction of the bond between C and O from a triple bond to a double bond to a single bond and eventually splitting C from O, in three steps: first between CO and formaldehyde (H₂CO), second between formaldehyde and methanol (CH₃OH) and finally between methanol and methane. We build upon and extend the diagram in Figure 2, where the temperature-and-pressure dependent pathways and RLSs are included, as explained in the following subsections.

3.1. CH₄-CO interconversion

3.1.1. Identifying the rate-limiting steps from full chemical kinetics

In addition to the RLS being a function of temperature and pressure, extracting this information to identify it is not straightforward because the possible number of paths grow exponentially with increasing number of species, making it

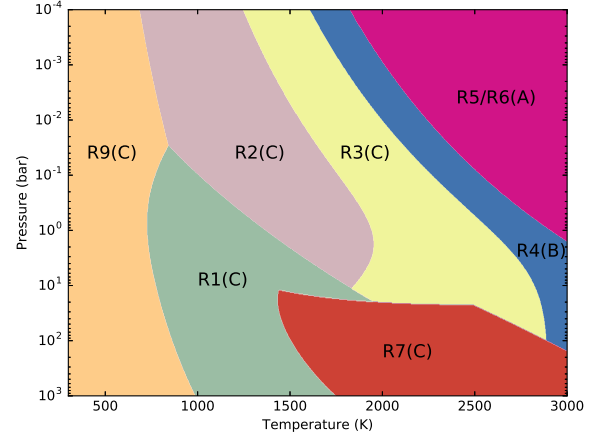
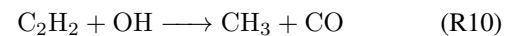
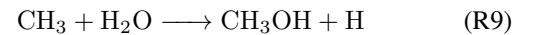
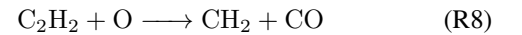
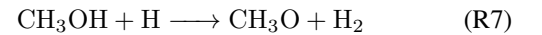
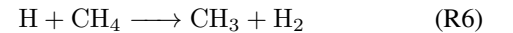
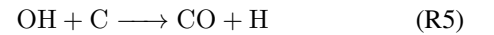
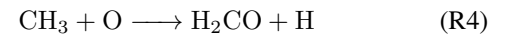
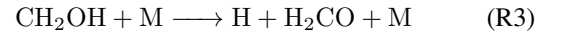
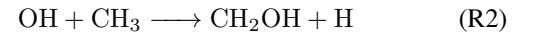


Figure 3. Parameter space of temperature and pressure showing how the rate-limiting step corresponds to different chemical reactions (R1 to R9; for more details, see text). These 9 chemical reactions may in turn be visualized as belonging to 3 different schemes (A, B and C; see text).

difficult to track them all. Our approach is to develop a tool using Dijkstra’s algorithm to find the shortest path and the associated RLS; see Appendix B for more details.

Figure 3 shows a survey of the different RLSs as functions of temperature and pressure and for protosolar elemental abundances from Lodders (2009) ($C/H = 2.776 \times 10^{-4}$, $O/H = 6.062 \times 10^{-4}$, $N/H = 8.185 \times 10^{-5}$, $He/H = 9.69 \times 10^{-2}$). Unsurprisingly, there does not exist a single RLS for the range of temperatures (500–3000 K) and pressures (0.1 mbar–1 kbar) considered. The different reactions, labeled R1 to R10, are



where M refers to any third body (i.e. the total number density of the gas). Reaction R8 and R10 are only relevant when $C/O > 1$, as we will describe shortly in the example of $C/O = 2$.

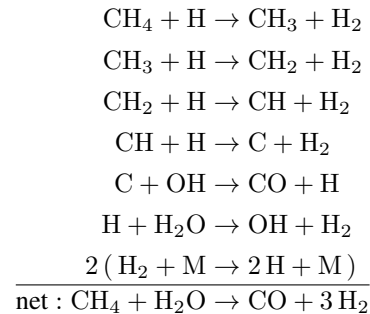
3.1.2. Grouping of reactions into three schemes

It is possible to understand CH_4 -CO interconversion as consisting of three schemes (at least, for solar-like elemental abundances). As temperature increases, the scheme moves from (C) to (A), as higher kinetic energy allows more ambitious steps.:

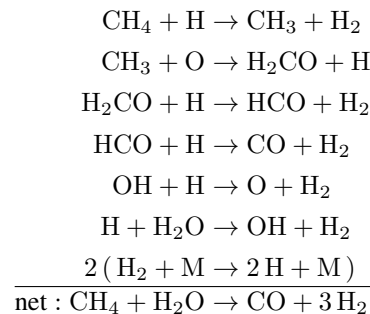
- (A): Though the progressive dehydrogenation of CH_4 into C, followed by oxidization into CO (blue arrows in Fig 2);
- (B): Via H_2CO (formaldehyde) from directly oxidizing CH_3 as described by (R4);
- (C): Via intermediate species like CH_2OH , CH_3OH , or CH_3O from oxidizing CH_3 (through the molecules shown in green in Fig 2).

At high temperatures and low pressures (the magenta region in Figure 3), scheme (A) is favored because it requires a high abundance of atomic hydrogen, produced mainly by thermal decomposition of H_2 . Scheme (B) sits in the transition between scheme (A) and (C). Scheme (C) covers the broadest range of temperature and pressure and contains the pathways previously identified by, e.g., Yung et al. (1988); Bézard et al. (2002); Moses et al. (2011); Visscher (2012). As shown in Figure 2, CH_4 is first converted to CH_3 before being oxidized by OH or H_2O to form CH_2OH or $\text{CH}_3\text{OH}/\text{CH}_3\text{O}$ depending on the temperature and pressure. These singly-bonded (C–O) intermediate species make forming the double bond (C=O) in H_2CO easier than directly from C and O. H_2CO goes on to efficiently produce HCO and finally the triple-bonded structure of CO. At high enough temperatures ($T \gtrsim 2000$ K), there is sufficient energy to directly form the double bond between C and O into H_2CO via reaction (R4) without passing through the intermediate species, which is scheme (B). This is similar to the RLS, $\text{CH}_3 + \text{OH} \rightarrow \text{H}_2 + \text{H}_2\text{CO}$, initially suggested by Prinn & Barshay (1977) to explain the quenched CO found in Jupiter. At even higher temperatures, if the pressure remains low enough then scheme (A) dominates. Molecular hydrogen is dissociated into atomic hydrogen, which in turn promotes the dehydrogenation of methane. Eventually, the accumulated C is present at high enough abundances that allow for its oxidization into CO.

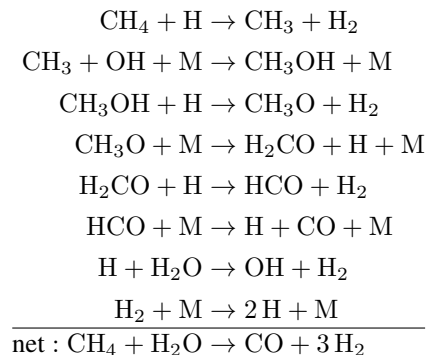
A typical pathway of scheme (A) is:



Scheme (B), which does not involve intermediate species like CH_3OH or CH_2OH , goes through the pathway:



Scheme (C) includes several main pathways for $T \lesssim 2000$ K or $P \gtrsim 1$ bar. One example of scheme (C) is:



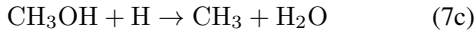
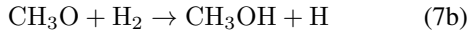
More examples of pathways belonging to scheme (C) may be found in Moses et al. (2011); Rimmer & Helling (2016); Tsai et al. (2017).

3.1.3. Comparison with previous work

Previous work studying CO- CH_4 interconversion has typically assumed one or two RLS, because their intentions were to estimate the location of the quench point (Yung et al. 1988; Lodders & Fegley 2002; Madhusudhan & Seager 2011; Visscher & Moses 2011). For the purpose of implementing chemical relaxation, this is insufficient. In Figure 4, we demonstrate this by comparing the calculations of chemical timescales associated with CH_4 and CO with those from Cooper & Showman (2006) and Visscher (2012). The discrepancies between our calculations and those from Visscher (2012) are mainly present at high temperatures and low pressures. There are significant discrepancies between our cal-

culations and the approximate ones by [Cooper & Showman \(2006\)](#) due to a different RLS assumed in [Cooper & Showman \(2006\)](#) as explained in the following paragraph. We use equation (16), instead of (19), of [Cooper & Showman \(2006\)](#), because the latter is an approximation that is valid only when $T \lesssim 2000$ K and the mole fraction of H_2 is close to 1. Instead of using equations (1) to (5) from [Cooper & Showman \(2006\)](#), we perform the full chemical-equilibrium calculations. We also include chemical timescales associated with NH_3 and N_2 for completeness.

[Cooper & Showman \(2006\)](#) consider a single $CO-CH_4$ pathway



proposed by [Yung et al. \(1988\)](#), where CO reacts with hydrogen to form H_2CO (formaldehyde) and goes through CH_3O (methoxide) and CH_3OH (methanol) to get to CH_3 (methyl). They suggested (7a), which is involved in breaking the $C=O$ bond, as being the RLS. [Cooper & Showman \(2006\)](#) adopt the rate constants from [Page et al. \(1989\)](#) and [Bézard et al. \(2002\)](#) for the low- and high-pressure limits, respectively. We verify that the rate coefficient from [Page et al. \(1989\)](#) has a value that is similar to what we use in our chemical network and is not the source of the discrepancies between our calculations and those of [Cooper & Showman \(2006\)](#).

Rather, the discrepancies stem from the rate coefficient associated with (7b), which had not been measured experimentally. [Yung et al. \(1988\)](#) assumed this reaction to be relatively fast, based on comparison with other similar reactions (see their Appendix A). Motivated by the importance of CH_3OH kinetics (see [Visscher et al. 2010](#) for details), [Moses et al. \(2011\)](#) performed ab initio calculations for the rate coefficients. According to their rate coefficients, (7b) always reacts slower than (7c) and thus should be the RLS ² We have chosen to use the rate coefficients of [Moses et al. \(2011\)](#).

[Visscher \(2012\)](#) identified (R1) and (R2) as being the RLSs and adopt the rate coefficients from [Jasper et al. \(2007\)](#). We have also taken the rate coefficients for (R1) from [Jasper et al. \(2007\)](#), but the reverse rate coefficient for (R2) from [Tsang \(1987\)](#). The differences between these rate coefficients are within a factor of 2. The two RLSs in [Visscher \(2012\)](#) control the most relevant temperature-pressure regions for hot/warm Jupiters ($\sim 1000 - 1500$ K) and their timescale agrees well with our calculation until entering the high-temperature and low-pressure regime.

² We also find this pathway suggested by [Yung et al. \(1988\)](#), except for (7b) being the RLS instead of (7a), becomes dominant at high pressures ($\gtrsim 100$ bar) and is important for Jupiter and Saturn where the CH_4-CO quench level is much deeper.

3.2. NH_3-N_2 interconversion

The timescales of nitrogen species are less constrained than that of CH_4-CO interconversion. HCN participates when $T \gtrsim 1000$ K and complicates the interconversion. We find it not straightforward to quantify the contribution of HCN and the real timescales deviate from those simply considering NH_3-N_2 interconversion.

The RLSs for NH_3-N_2 interconversion are

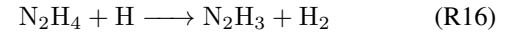
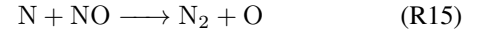
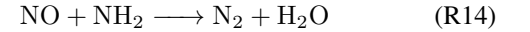
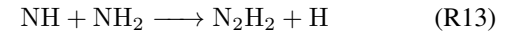
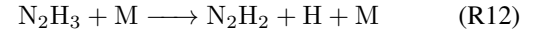
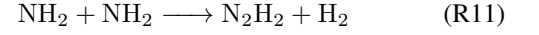
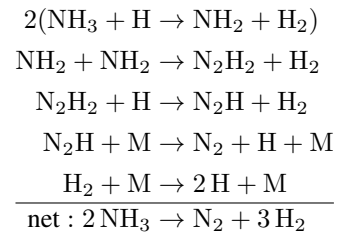


Figure 5 visualizes the network of RLSs for nitrogen chemistry, while Table 1 lists the RLSs of NH_3-N_2 , across temperature and pressure.

NH_3-N_2 interconversion can be divided into two schemes, depending on whether N_2 is formed from N_2H or NO . At high pressures (the parameter space occupied by (R11), (R12), and (R13) in Table 1), N_2 is mainly formed by the dissociation of N_2H , with a pathway such as



where the second reaction (R11) is the RLS. As temperature increases, (R11) is replaced by (R13), or a channel through N_2H_3 and N_2H_4 (R12). This pathway is similar to that identified for HD 209458b by [Moses et al. \(2011\)](#).

At low pressures (the parameter space occupied by (R14) and (R15) in Table 1), H_2 is attacked by the more abundant free atomic O and produces OH, which in turn forms NO with N via $N + OH \rightarrow NO + H$. NO then react with N or NH_2 , depending on the temperature, to produce N_2 . This step involves forming the $N \equiv N$ bond and is usually the RLS.

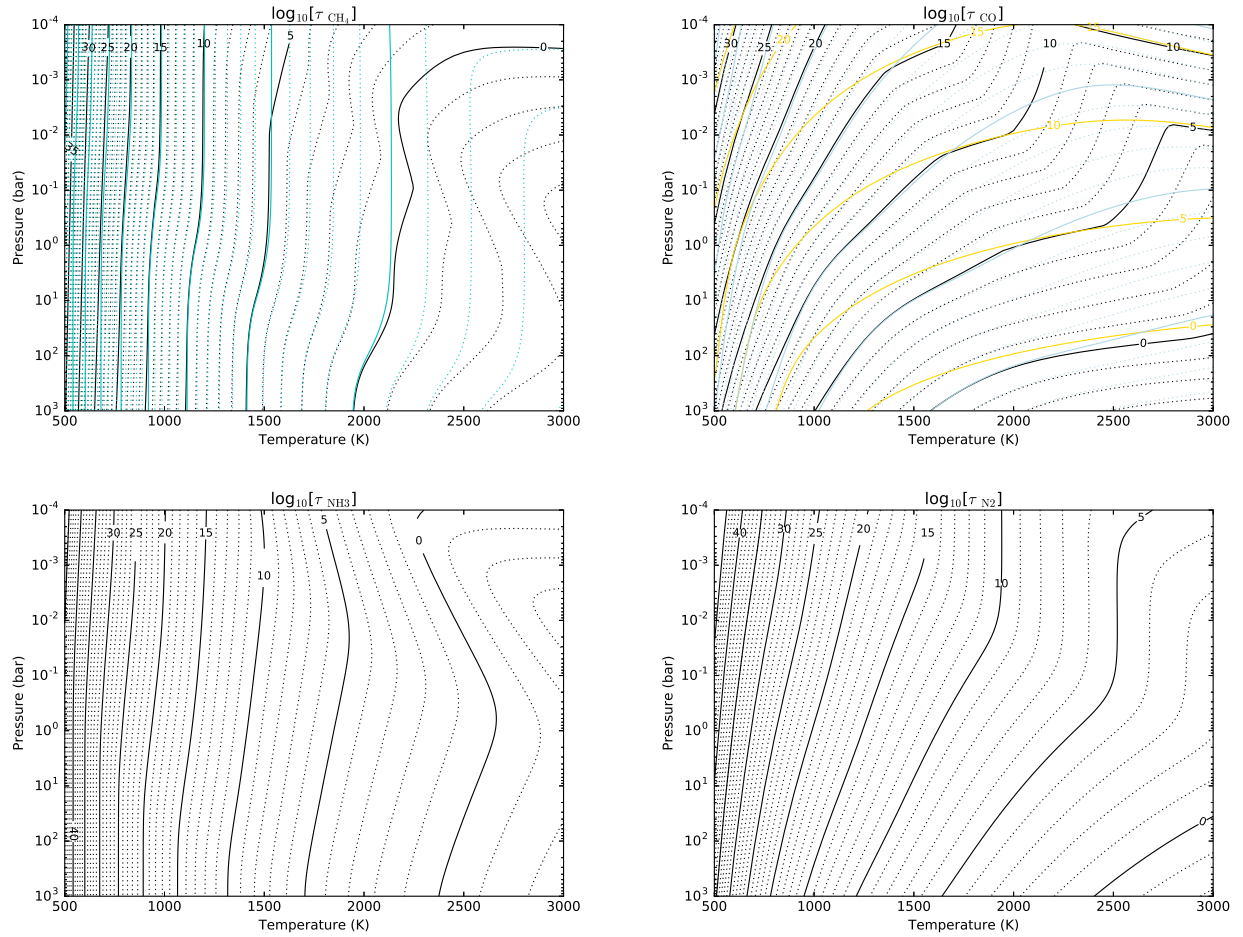


Figure 4. Chemical timescales associated with the production of CH_4 , CO , NH_3 and N_2 as functions of temperature and pressure. The black curves are our calculations, while the cyan curves are from [Visscher \(2012\)](#) (for CH_4 and CO) and the yellow curves are from [Cooper & Showman \(2006\)](#) (for CO).

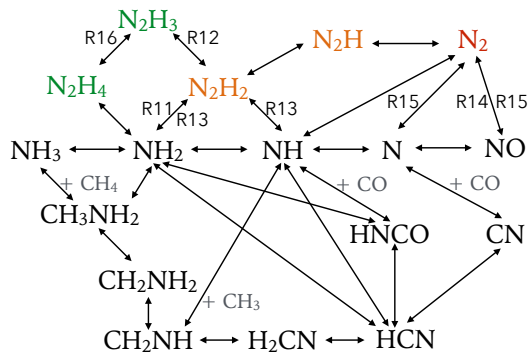
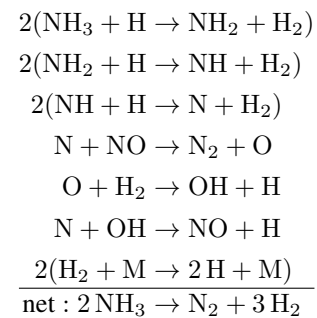


Figure 5. Schematic illustration as Figure 2 but for the major chemical pathways between NH_3 , N_2 , and HCN .

The pathway becomes



where (R15) is the RLS.

4. COMPUTING CHEMICAL TIMESCALES

The full expressions for the chemical timescales, including those involving methane, carbon monoxide, water, ammonia and molecular nitrogen, are stated in [Appendix A](#). In the following, we explain the reasoning behind their construction.

4.1. Revisiting CH_4 - CO interconversion

The study of interconversion between methane and carbon monoxide has a long and rich history. In the current study, we

Table 1. $\text{NH}_3 \leftrightarrow \text{N}_2$ rate-limiting reactions

T (K)	500	1000	1500	2000	2500
P (bar)					
10^{-4}	R11	R14	R15	R15	R15
10^{-3}	R11	R14	R13	R15	R15
10^{-2}	R11	R13	R13	R15	R15
10^{-1}	R11	R12	R13	R13	R15
1	R12	R12	R13	R13	R13
10	R11	R12	R13	R13	R13
100	R11	R12	R16	R13	R13

Table 2. $\text{CH}_4 \leftrightarrow \text{CO}$ rate-limiting reactions (solar abundance)

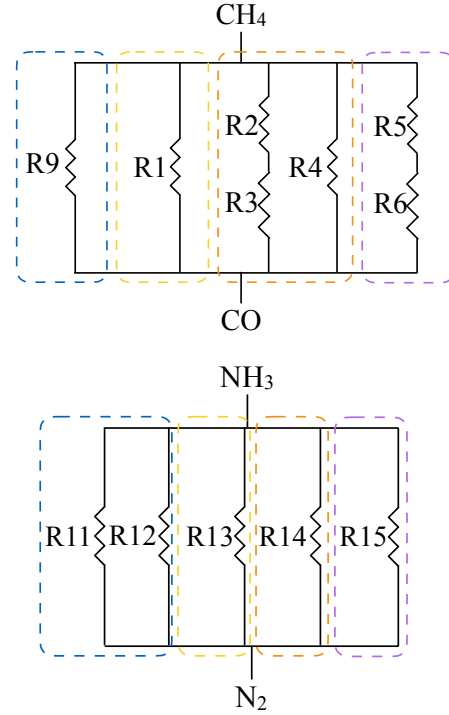
T (K)	500	1000	1500	2000	2500
P (bar)					
10^{-4}	R9	R2	R3	R5	R6
10^{-3}	R9	R2	R3	R4	R5
10^{-2}	R9	R2	R2	R4	R5
10^{-1}	R9	R1	R2	R3	R4
1	R9	R1	R2	R3	R3
10	R9	R1	R1	R3	R3
100	R9	R1	R1	R7	R7

Table 3. $\text{CH}_4 \leftrightarrow \text{CO}$ rate-limiting reactions ($\text{C/O} = 2$)

T (K)	500	1000	1500	2000	2500
P (bar)					
10^{-4}	R9	R2	R8	R8	R5
10^{-3}	R9	R2	R8	R8	R8
10^{-2}	R9	R2	R10	R8	R8
10^{-1}	R9	R1	R2	R8	R8
1	R9	R1	R2	R3	R8
10	R9	R1	R1	R3	R8
100	R9	R1	R7	R7	R7

focus on identifying the pathways in reducing atmospheres, while the same steps can be applied to other types of atmospheres. In this subsection, our goal is to provide an analytical expression for computing the timescale associated with CH_4 -CO interconversion as a function of the reactions (R1) to (R10). Table 2 shows the RLSs for solar metallicity, while Table 3 shows them for $\text{C/O} = 2$. Reactions (R8) and (R10) are only relevant for $\text{C/O} = 2$, as previously mentioned.

Under differing conditions of temperature and pressure, the various RLSs can either collaborate or compete with one another. We find that a useful analogy for understanding the pathways is to visualize them as the resistors in an electrical circuit—built in series or in parallel. Using such an analogy, we can construct an analytical expression for the chemical

**Figure 6.** The effective “electronic circuit” of the major chemical pathways between methane and carbon monoxide (upper) for Figure 2 and between ammonia and molecular nitrogen (lower) for Figure 5. The dashed rectangles in blue, yellow, orange, and purple group the RLSs according to their operating temperatures and pressures.

timescale that consists of a network of reactions working either in series or in parallel. The upper diagram of Figure 6 visualizes how such an analogous electrical circuit would look like for CH_4 -CO interconversion. We identify the series and parallel RLSs and group the RLSs that operate in similar temperatures and pressures together. For example, (R2), (R3) are in series but (R2) and (R4) are in parallel. Depending on the temperature and pressure, either (R1), (R9), or the group of (R2), (R3), and (R4) is in control.

Mathematically, a pair of reactions in parallel can be expressed as an operation that takes the maximum of the two rate coefficients. For a pair of reactions in series, the operation instead takes the minimum of the two rate coefficients. The groups that operate in particular temperatures and pressures are then added together for simplicity. In this way, the series of relationships between the reactions can be expressed as

$$\tau_{\text{CH}_4} = \frac{[\text{CH}_4]}{r1 + \max(\min(r2, r3), r4) + r9 + \min(r5, r6)} + \tau_{\text{H}_2} \times \frac{3[\text{CO}]}{[\text{H}_2]}, \quad (10)$$

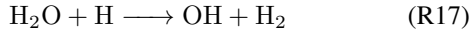
where $[\text{X}]$ represents the equilibrium number density of species X in cm^{-3} , rx stands for the reaction rate of (Rx), and the factor $\frac{3[\text{CO}]}{[\text{H}_2]}$ stems from the amount of hydrogen that participates in the CH_4 -CO interconversion (three H_2 for every

CO according to the net reaction). The second term is usually orders of magnitude smaller than the first term except at high temperatures and low pressures, where the dissociation and recombination between H and H₂ become important and the relatively slower conversion of hydrogen starts to bottleneck the process. We demonstrate how methane is controlled by hydrogen in Figure B2 where we manually vary the rate of H-H₂ dissociation/recombination.

We have also replaced (R7) with (R1) for simplicity because the rates of both reactions are very similar at high pressures. The same formula is applied to τ_{CO} except one needs to replace the numerator with [CO], since the interconversion goes both ways.

4.2. Water

H₂O reacts efficiently with atomic hydrogen via

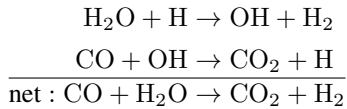


in a hydrogen-rich atmosphere. Being the major oxygen carrier, water prevalingly participates in various reaction pathways, e.g. CO \leftrightarrow CO₂ and H₂ \leftrightarrow 2H. For solar metallicity, carbon is the richest heavy element next to oxygen. We find the timescale of water is effectively determined by the interconversion rate of CH₄-CO,

$$\begin{aligned} \tau_{\text{H}_2\text{O}} = & \frac{[\text{H}_2\text{O}]}{r1 + \max(\min(r2,r3), r4) + r9 + \min(r5,r6)} \\ & + \tau_{\text{H}_2} \times \frac{3[\text{CO}]}{[\text{H}_2]}. \end{aligned} \quad (11)$$

4.3. Carbon dioxide

Carbon dioxide is produced through the relatively fast scheme (Line et al. 2010; Moses et al. 2011)



The chemical timescale is simply

$$\tau_{\text{CO}_2} = \frac{[\text{CO}_2]}{k_{\text{CO}_2}[\text{CO}][\text{OH}]} \quad (12)$$

where k_{CO_2} is the rate coefficient for CO + OH \longrightarrow CO₂ + H. Due to the fast conversion, CO₂ still maintains pseudo-equilibrium with CO and H₂O after the latter two are quenched, before CO₂ reaches its own quench point (see the discussion in section 3.1 of Moses et al. 2011). Owing to this coupling, instead of relaxing CO₂ to its equilibrium value, we find it correct to relax CO₂ toward the pseudo-equilibrium value determined by the (possibly quenched) CO and H₂O, as expressed in equation (A7), similar to the treatment in equation (43) of Zahnle & Marley (2014).

4.4. Ammonia and molecular nitrogen

The chemical timescale of ammonia is approximately determined by the NH₃-N₂ conversion. Omitting HCN, we group the RLSs with similar operating temperatures and pressures and construct the effective electrical circuit in the lower diagram of Figure 6.

For ammonia production, we have

$$\tau_{\text{NH}_3} = \frac{1}{2} \left(\frac{[\text{NH}_3]}{\max(r11,r12) + r13 + r14 + r15} + \tau_{\text{H}_2} \times \frac{3[\text{N}_2]}{[\text{H}_2]} \right) \quad (13)$$

where the factor $\frac{3[\text{N}_2]}{[\text{H}_2]}$ is again the amount of hydrogen that participates in the NH₃-N₂ interconversion, as in the CH₄-CO interconversion limited by H-H₂ interconversion at high temperatures and low pressures, and the factor of 1/2 comes from the fact that the net reaction converts two NH₃ molecules to one N₂ molecule.

Following the same steps, the chemical timescale of molecular nitrogen is expressed as

$$\tau_{\text{N}_2} = \frac{[\text{N}_2]}{\max(r11,r12) + r13 + r14 + r15} + \tau_{\text{H}_2} \times \frac{3[\text{N}_2]}{[\text{H}_2]} \quad (14)$$

4.5. The effects of metallicity

As the metallicity is varied from 10⁻² × to 1000 × of the solar values, we find that the chemical pathways and RLSs discussed in section 3 do not change. Therefore, the formulae for the timescales remain the same. An exception is for the NH₃-N₂ pathways as the metallicity approaches 100 × solar. (R14) and (R15) occupy more of the temperature-pressure parameter space because of the richness of oxygen. We also confirm that τ_{CO} is almost independent of metallicity and τ_{CH_4} is inversely proportional to metallicity, as found by Visscher (2012).

Once the metallicity increases beyond 1000 × solar, the atmosphere ceases to be H₂-dominated and the main constituents become carbon dioxide or molecular oxygen (Hu & Seager 2014). For example, at 10⁴ × solar metallicity, CH₄ becomes scarce simply because of the lack of hydrogen for its formation. In this scenario, CO-CO₂ interconversion becomes the main quenching process and follows the same pathway as for solar metallicity with the timescale still given by equation (12). The pathways involving the nitrogen species become completely altered. Generally, the reactions of NH_x with H₂O become important in controlling NH₃-N₂ interconversion.

4.6. The effects of C/O

The carbon-to-oxygen ratio (C/O) is a crucial factor in controlling the atmospheric chemistry and thermal structure (Madhusudhan 2012; Moses et al. 2013a; Venot et al. 2015; Rocchetto et al. 2016). Equilibrium chemistry is sensitive to C/O and undergoes a qualitative transition at C/O = 1. We explore C/O values ranging from 0.1 to 2. The reason to limit

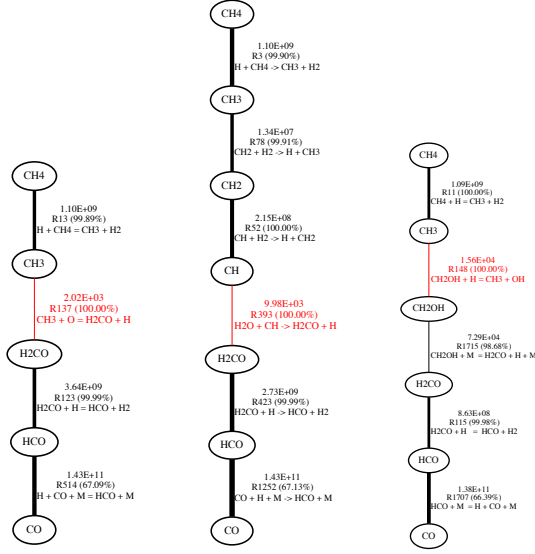
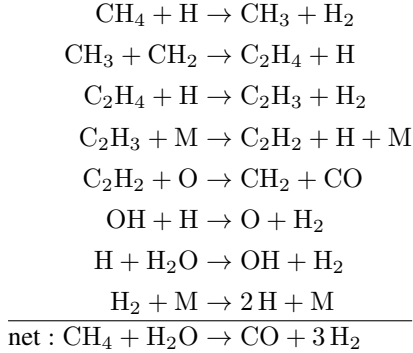


Figure 7. Examples of CH_4 -CO pathway analysis at $T = 2000$ K and $P = 0.1$ bar with the chemical network from VULCAN (left), Moses et al. (2011) (middle), and Venot et al. (2012) (right). Thicker lines represent faster reaction rates (denoted by the first-row numbers shown in $\text{cm}^{-3}\text{s}^{-1}$ and the percentage of contribution to the interconversion rate is also provided) and the red lines are the rate-limiting steps.

ourselves at $C/O = 2$ is that C/O much larger than unity is considered unlikely as the surplus carbon tends to condense and form graphite (Moses et al. 2013b). Comparing Table 2 and Table 3, the major change as C/O exceeds unity is carbon takes the route through C_2H_2 at high temperature. The typical pathway in a hot, carbon-rich atmosphere is



where $\text{C}_2\text{H}_2 + \text{O} \rightarrow \text{CH}_2 + \text{CO}$ (R8) is the RLS in the above pathway. The corresponding timescale for C/O between 1 and 2 is

$$\tau_{\text{CH}_4} = \frac{[\text{CH}_4]}{r1 + \min(r2,r3) + r9 + \max(r8,r10)}, \quad (16)$$

In this scheme, CH_4 -CO conversion is no longer limited by hydrogen dissociation.

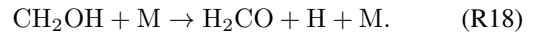
5. COMPARISON OF CHEMICAL NETWORKS USING PATHWAY ANALYSIS

We recognize that the chemical pathways taken depend entirely on the network one is using. With a different net-

work, the rate-limiting chemical reactions need to be re-identified. The expressions for chemical timescales can be worked out following the same steps in §4. Here, we compare our network with two others that have included high-temperature chemical kinetics and been applied to hot exoplanets. We first compare our network with that of Moses et al. (2011); our two networks are naturally similar, because we have taken the values of certain rate coefficients from that study. We then compare our network with that of Venot et al. (2012). In Figure 7, we use our pathway analysis tool to compare the route taken by each network (Since the reaction rates are calculated with equilibrium composition, the forward rate equals to the reverse rate, there is no directionality in the pathways, i.e. $\text{CH}_4 \rightarrow \text{CO}$ takes the same pathway as $\text{CO} \rightarrow \text{CH}_4$).

At solar abundance and temperatures less than 2000 K, the network of Moses et al. (2011) shows almost exactly the same CH_4 -CO pathways as ours. Due to a different choice of the rate coefficients associated with (R2), part of the parameter space occupied by (R3) is replaced by (R2) in their network for $T \gtrsim 2000$ K and $P \sim 10$ bar. (R7) also extends to lower pressures in their network. At high temperatures and low pressures in scheme (A), their network experiences the same dehydrogenation process, but instead of (R4) and (R5), their network chooses a faster path through water: $\text{CH} + \text{H}_2\text{O} \rightarrow \text{H}_2\text{CO} + \text{H}$ (which is not included in our network). Yet, in this regime, the timescale is limited by hydrogen dissociation and yields the same timescale of CH_4 -CO interconversion as we do. At $C/O = 2$, carbon forms abundant C_2H_2 and then gets oxidized to CO in a similar way, but except via (R10), it takes $\text{C}_2\text{H}_2 + \text{OH} \rightarrow \text{H}_2\text{CCO} + \text{H}$ or $\text{C}_2\text{H}_2 + \text{O} \rightarrow \text{HCCO} + \text{H}$ in their network. H_2CCO or HCCO then proceeds to be split into CO by H. In general, our network is consistent with that of Moses et al. (2011), as suggested by the comparison in Tsai et al. (2017).

The overall CH_4 -CO timescale in Venot et al. (2012) is shorter than ours and Moses et al. (2011). We find the two key reactions that make the RLSs and essentially the timescales different are (R9) and



Venot et al. (2012) includes faster rate coefficients for both (R9) and (R18). Their rate coefficient for (R9) is based on the work of Hidaka et al. (1989), which has been suggested as overestimating the rate; see discussion in Visscher (2012) and Moses (2014). This rate coefficient is significantly higher (~ 10 orders of magnitudes) than the ab initio calculation in Moses et al. (2011), which is also used in our network.

At lower temperatures ($T \lesssim 1000$ K), Venot et al. (2012) takes the same pathway through (R9), forming CH_3OH from CH_3 and H_2O . However, with a faster rate it never bottlenecks the pathway and controls the timescale. Their RLSs are instead the reactions involving forming or destroying H_2CO ,

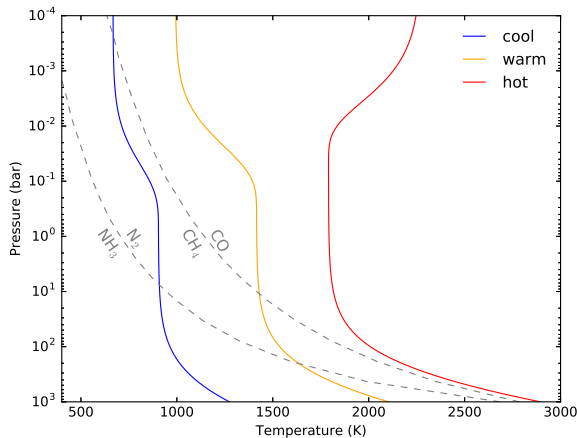


Figure 8. Representative temperature-pressure profiles representing hot, warm, and cool atmospheres. Gray dashed curves show the boundaries where $\text{CH}_4\text{-CO}$ and $\text{NH}_3\text{-N}_2$ have equal abundances in chemical equilibrium.

e.g. $\text{CH}_3\text{O} + \text{M} \rightarrow \text{H}_2\text{CO} + \text{H} + \text{M}$ and $\text{H}_2\text{CO} + \text{H} \rightarrow \text{HCO} + \text{H}_2$. Similarly, due to the faster $\text{CH}_3\text{-CH}_3\text{OH}$ channel via (R9), for $1000 \text{ K} \lesssim T \lesssim 1500 \text{ K}$, Venot et al. (2012) exhibits pathways close to ours, except that our (R1) is replaced by $\text{CH}_2\text{OH} + \text{H}_2 \rightarrow \text{CH}_3\text{OH} + \text{H}$ as the RLS. At higher temperature where $T \gtrsim 1500 \text{ K}$, the differences are mainly attributed to (R18). Venot et al. (2012) uses the rate from Greenhill et al. (1986), validated for 600–1000 K, while this work and Moses et al. (2011) use the rate from Cribb et al. (1992), validated for 1900–2700 K. The former is about two orders of magnitude larger than the latter in this temperature range. Consequently, the fast $\text{CH}_2\text{OH-H}_2\text{CO}$ interconversion in Venot et al. (2012) again never limits the pathway (e.g. the right pathway in Figure 7). Their RLS remains $\text{CH}_2\text{OH} + \text{H}_2 \rightarrow \text{CH}_3\text{OH} + \text{H}$ for high pressures and switches to $\text{CH}_3 + \text{OH} \rightarrow \text{CH}_2\text{OH} + \text{H}$ for low pressure.

In conclusion, our pathway analysis tool is useful in identifying the key reactions for a given network, which allows us to diagnose the divergent behaviors of different networks. By isolating the rate coefficients of the key reactions involved, we hope to motivate future laboratory and/or theoretical studies that will hopefully resolve these discrepancies.

6. VALIDATION OF CHEMICAL RELAXATION METHOD

We are finally ready to validate the chemical relaxation method to a factor of several, having assembled the necessary ingredients.

6.1. Setup

The goal of any chemical calculation, either from full kinetics or any simplified method, is to provide the rate of change of every species locally. The applicability of the relaxation method should not depend on the format or complexity of atmospheric dynamics. Therefore, before including the chemical relaxation method in a GCM, we evaluate

whether and to what extent the relaxation method can replace full chemical kinetics with a one-dimensional full kinetics model, where eddy diffusion (K_{zz}) is used to represent vertical mixing. For w (vertical velocity) $\sim 1 \text{ km s}^{-1}$ and $H \sim 100 \text{ km}$, we have $K_{zz} \lesssim wH \sim 10^{12} \text{ cm}^2 \text{ s}^{-1}$. To exaggerate the effects of vertical mixing, we explore a range of K_{zz} values up to $10^{15} \text{ cm}^2 \text{ s}^{-1}$.

We run the same atmospheric conditions with the relaxation method and VULCAN, a full kinetics model with a C-H-O network including 29 species with up to two carbon atoms and about 300 forward and reverse reactions (Tsai et al. 2017). For nitrogen chemistry, an updated N-C-H-O network is implemented including 53 species and about 600 forward and reverse reactions. The chemical equilibrium abundances are calculated using the FastChem (Stock et al. 2018) code. We perform our chemistry calculations over three temperature-pressure profiles constructed using the analytical formula in Heng et al. (2014) to represent cool, warm and hot atmospheres (Figure 8). These profiles are meant to mimic GJ 1214b-, HD 189733b- and WASP-18b-like atmospheres. With the atmospheres we tested, the computational time for integrating one step using the chemical relaxation method is about 5 ms, compared to about 0.5 s using VULCAN. The computational speed can be increased by about 100 times with the chemical relaxation method.

6.2. Hot atmospheres (WASP-18b-like)

At solar metallicity and high temperatures, CO, H_2O , and N_2 are the dominant molecules in chemical equilibrium (Madhusudhan 2012; Moses et al. 2011; Heng & Tsai 2016). In Figure 9, it is therefore unsurprising that the mixing ratios of the first two molecules (not showing N_2) are insensitive, or nearly independent of, pressure. For $K_{zz} \lesssim 10^{13} \text{ cm}^2 \text{ s}^{-1}$, the mixing ratios of CO and H_2O essentially track their chemical-equilibrium values closely, deviating only with stronger mixing and/or lower pressures ($\lesssim 1 \text{ mbar}$).

The mixing ratios of CH_4 and NH_3 exhibit a much larger range of values as they both drop off significantly with increasing altitude: 13 and 7 orders of magnitude for CH_4 and NH_3 , respectively, over the range of pressure examined (0.1 mbar to 1 kbar). Over these broad ranges, the chemical relaxation method performs fairly well, exhibiting an accuracy of within an order of magnitude for the most part. With strong vertical mixing, CH_4 and NH_3 begin to quench at about 10 bar and 100 bar, respectively. At about 1 mbar, hydrogen dissociation/recombination slows down the interconversion and sets the second quench level. If the effect of hydrogen dissociation is neglected, the estimated chemical timescale will be too short and the prediction of CH_4 and NH_3 will be too close to chemical equilibrium.

6.3. Warm atmospheres (HD 189733b-like)

Figure 10 shows the mixing ratios of CO, CO₂, CH₄, H₂O and NH₃ for a HD 189733b-like atmosphere. The chemical relaxation method performs with an accuracy of better than a factor of 2 in most parts across a broad range of pressures and mixing ratio values, with NH₃ being least accurate due to the error in estimating its timescale. For comparison, we show the chemical-relaxation calculations performed using our implementation of the method of Cooper & Showman (2006) as dot-dashed curves. Recall that Cooper & Showman (2006) uses essentially a shorter single chemical timescale of CO (tied to a single RLS), whereas the main goal of the present study is to use a set of rate-limiting chemical reactions depending on the temperature and pressure conditions to obtain more accurate timescales.

Cooper & Showman (2006) and Drummond et al. (2018) only calculate CO using the relaxation method and relate CH₄ (and other species) through mass balance, assuming that all the carbons are locked in either CH₄ and CO, hence the mixing ratios X_{CH_4} and X_{CO} are conserved:

$$X_{\text{CH}_4} + X_{\text{CO}} = C/(\text{H}_2 + \text{He}) \quad (17)$$

where $C/(\text{H}_2 + \text{He})$ is the ratio of carbon atoms to molecular hydrogen and helium (i.e. the bulk gas), determined by solar metallicity. We emphasize that this mass balance relation is only valid when (1) the system is in or close to chemical equilibrium (2) temperature is not too high such that all hydrogen remains in molecular form (3) CH₄ and CO have close abundances. The elemental abundance ($C/(\text{H}_2 + \text{He})$ in this case) is a local property, and can be violated by disequilibrium processes³. We demonstrate this in the top right panel in Figure 10, with the mixing ratios of CH₄ calculated from equation (17) using X_{CO} obtained from chemical relaxation (the top left panel in Figure 10) in dot-dashed curves. The mass balance approach overpredicts the quenching of CH₄. Furthermore, as CO is ~ 3 orders of magnitude more abundant than CH₄ in this case, which requires the estimation of CO to be as accurate as ~ 3 decimal places for the mass balance approach to work. Unfortunately, this precision is not attainable with the relaxation method or any other kinetics models. Therefore, the mass balance approach can only be applied to a system in chemical equilibrium but not applicable to the relaxation method.

For CO₂, we show for comparison the calculation of relaxing CO₂ to the equilibrium abundance of CO₂ (dot-dashed curves) versus to its pseudo-equilibrium value as determined by the quenched abundances of CO and H₂O (solid curves). The difference in accuracy is substantial: $\sim 10\%$ versus an order of magnitude. Neglecting this effect will lead to the inaccurate prediction that the mixing ratio of CO₂ is close to

equilibrium.

For illustration, we show the mixing ratios of CH₄ when the metallicity is $100\times$ solar, as well as those of H₂O and CO₂ when $C/O = 2$. In the latter case, H₂O loses its dominance to CH₄ and its mixing ratio becomes sensitive to the strength of vertical mixing. In these cases, our more general treatment of chemical relaxation allows the accuracy of the method to remain about the same as for the solar-metallicity case.

6.4. Cool atmospheres (GJ 1214b-like)

Figure 11 shows the mixing ratios of CO, CO₂, CH₄ and N₂ for a GJ 1214b-like atmosphere. In this range of temperatures, the chemical relaxation method is highly accurate ($\sim 10\%$). For CO, the difference from using the single-RLS timescale of Cooper & Showman (2006) increases significantly to a few orders of magnitudes. However, we note that photochemistry will potentially influence the abundances in these cooler atmospheres, which is not taken into account in this work.

7. SUMMARY AND DISCUSSION

7.1. Summary

Inspired by the pioneering work of Cooper & Showman (2006), we have revisited the chemical relaxation method, which seeks to greatly enhance computational efficiency by replacing the network in a chemical kinetics calculation with a few independent source/sink terms that “relax” towards chemical equilibrium on a prescribed timescale. There is a precedent of using relaxation methods as a substitute for radiative transfer, where the timescale is then associated with radiative cooling (e.g., Held & Suarez 1994). The main lessons learned from our study are:

- The rate-limiting reaction that determines the chemical timescale depends on the temperature and pressure. For CH₄-CO and NH₃-N₂-HCN interconversion, we show across a broad range in temperature and pressure (500–3000 K, 0.1 mbar to 1 kbar) that there are multiple rate-limiting reactions, and that the chemical timescale cannot be easily fitted by an Arrhenius-like function.
- By comparing full chemical-kinetics to chemical-relaxation calculations in one dimension, we show that the latter is accurate to within an order of magnitude for WASP-18b-like atmospheres, \sim a factor of 2 for HD 189733b-like atmospheres and $\sim 10\%$ for GJ 1214-b-like atmospheres. Essentially, the chemical relaxation method is more accurate when the species either fully quench or retain chemical equilibrium. The discrepancies become larger when the species do not fully quench, because the behavior is more sensitive to the timescale in this situation. Overall, species at

³ For example, CO quenching alone increases the metallicity relative to that in chemical equilibrium, although the effect of changing the metallicity is usually small since the quenched species are trace gases.

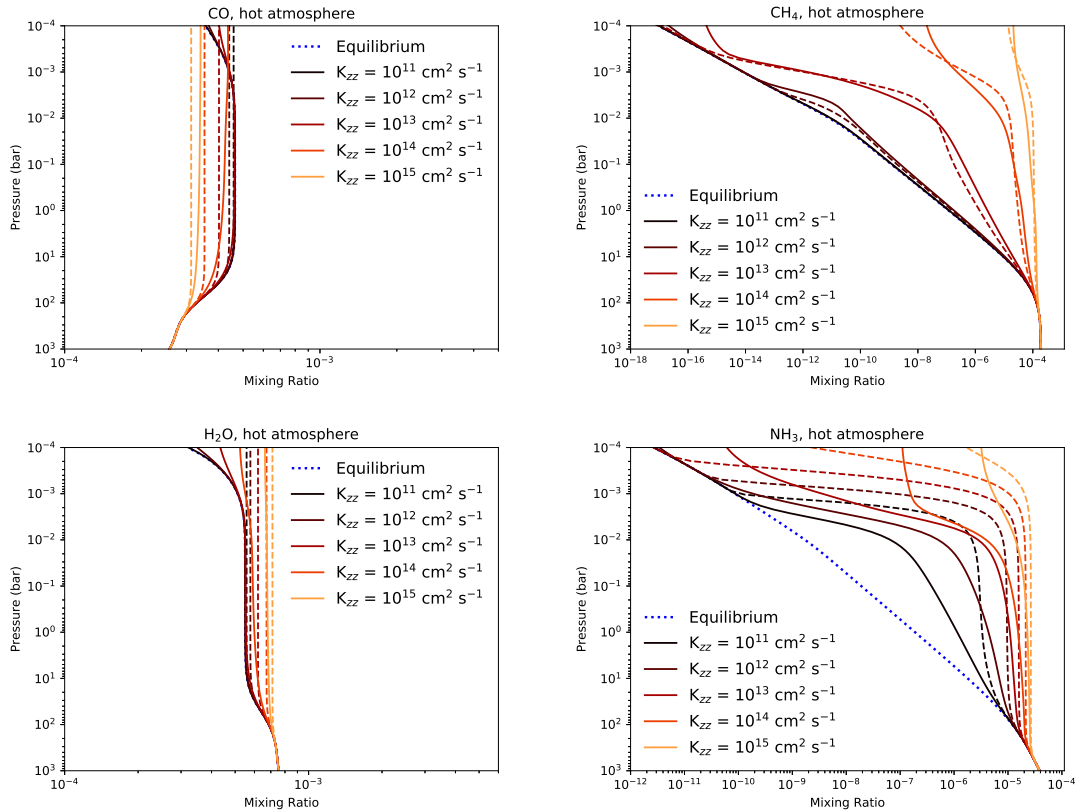


Figure 9. Mixing ratios of CO, CH₄, H₂O, and NH₃ in the hot atmosphere as displayed in Figure 8. The results of the relaxation method (dashed) are compared to the full chemical kinetics (solid) for a range of vertical mixing strengths shown in various colors. The mixing ratio in chemical equilibrium is shown as a dotted curve.

lower temperatures tend to fully quench (e.g., Moses et al. 2016) since the timescale of the main quenched species (CO and N₂) quickly increases with altitude (see Figure 4). This bodes well as the currently characterizable atmospheres will become cooler as observational methods advance, but the effects of photochemistry need to be examined.

- The relaxation method increases the computational speed by at least 100 times compared to running a full kinetics model. More importantly, the relaxation method allows decoupling from the chemical network. Only the species of interest need to be included, which will significantly ease the burden of adding numerous tracers to the dynamical core.

7.2. Opportunities for future work

There are ample opportunities for future work. We have recently finished and submitted the work of coupling our chemical relaxation method to our GCM (Mendonça et al. 2016)

and studying the interaction between atmospheric dynamics and chemistry in three dimensions. It remains an open question if photochemistry may be reasonably approximated by chemical relaxation, since it will require a pre-calculated photochemical steady state for a given atmospheric condition and stellar flux. Generalizing chemical relaxation to work in the regime of atmospheres with Earth-like temperatures will be useful as we march towards the study of exo-climates similar to our own.

S.-M.T. and K.H. acknowledge partial financial support from the PlanetS National Center of Competence in Research (NCCR), the Center for Space and Habitability, the Swiss National Science Foundation and the Swiss-based MERAC Foundation, as well as useful conversations with Julie Moses and Paul Rimmer.

Software:

Python⁴, SciPy⁵, NumPy⁶ (van der Walt et al. 2011), Matplotlib⁷ (Hunter 2007)

⁴ <http://www.python.org>

⁵ <http://scipy.org>

⁶ <http://numpy.org>

⁷ <http://matplotlib.org>

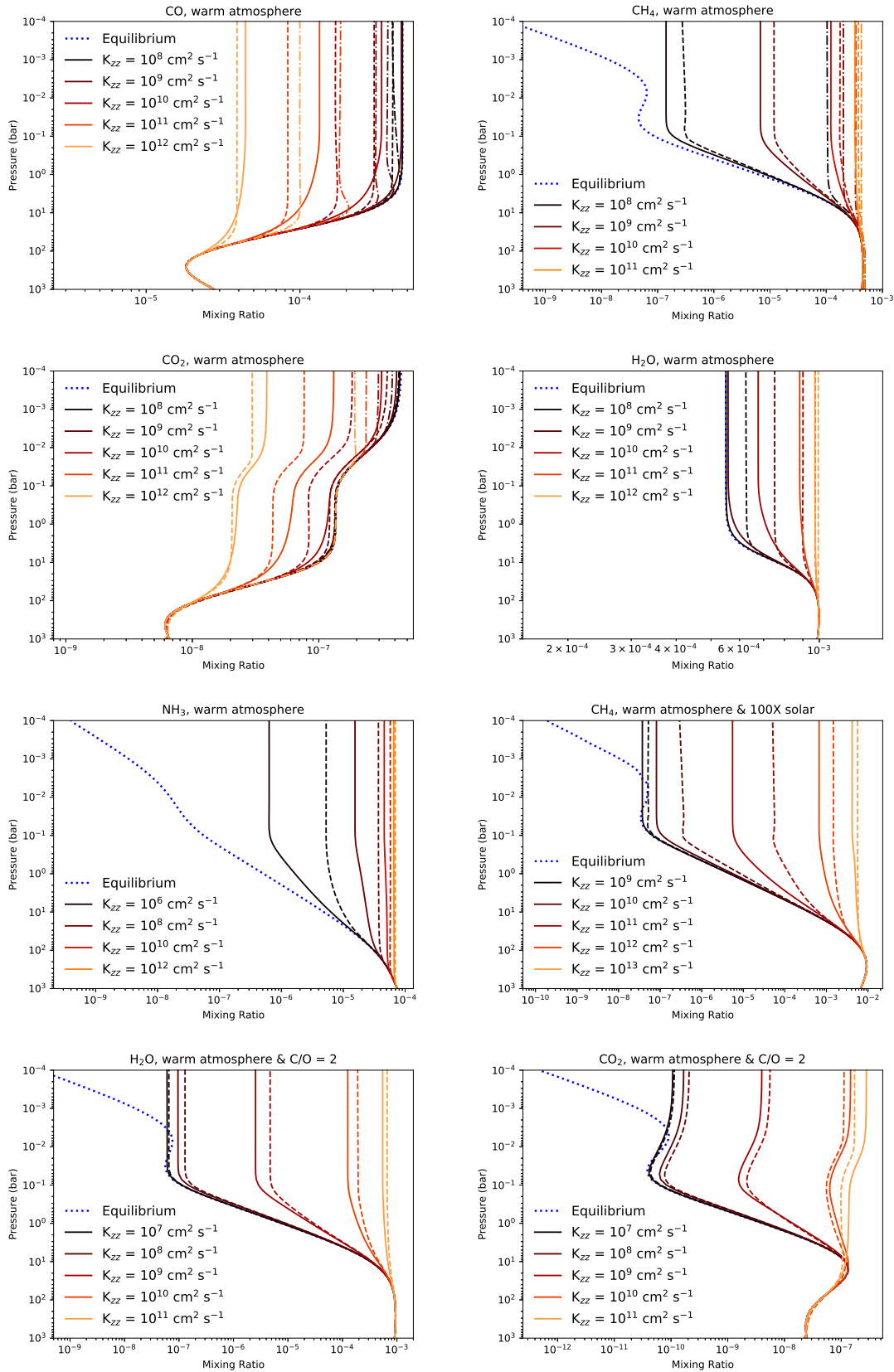


Figure 10. Same as Figure 9 but for the warm atmosphere. For CO, the chemical-relaxation calculations adopting the timescale from Cooper & Showman (2006) are shown as dashed-dotted curves. For CH₄, the mass balance approach using the chemical-relaxation calculations of CO are shown in dashed-dotted curves. For CO₂, the chemical-relaxation calculations without considering the coupling to CO and H₂O are shown in dashed-dotted curves for comparison.

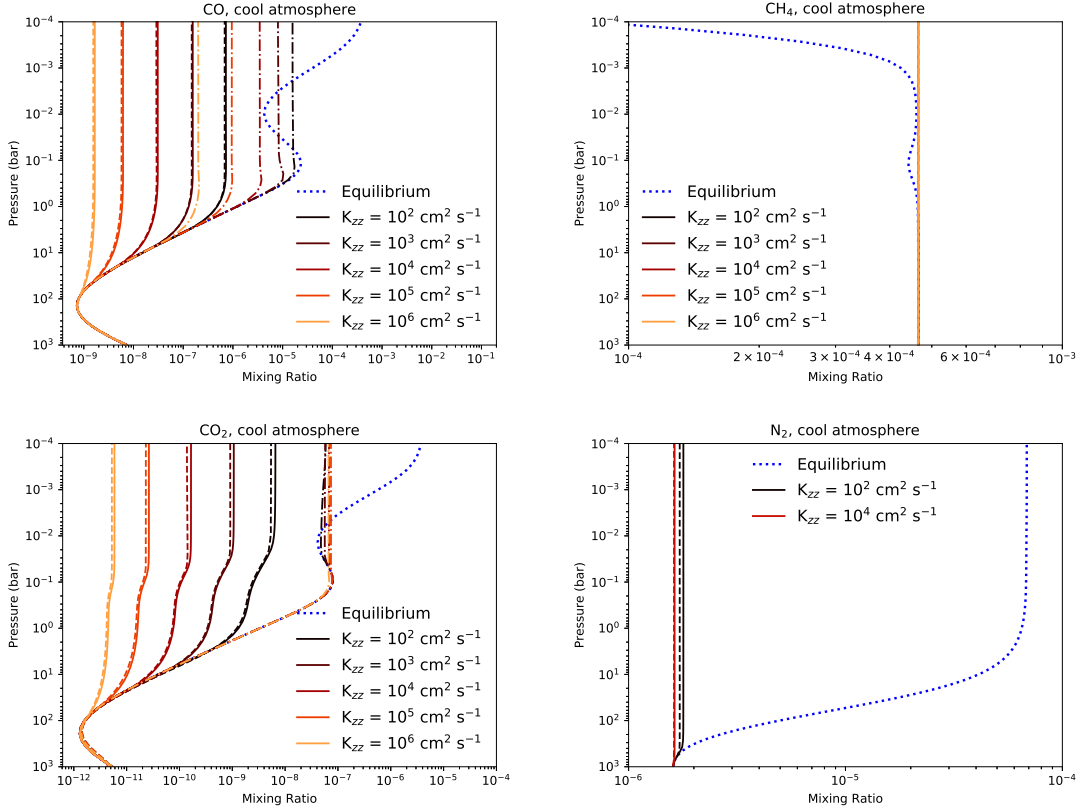


Figure 11. Same as Figure 9 but for the cool atmosphere. For CO, the chemical-relaxation calculations adopting the timescale from Cooper & Showman (2006) are shown as dashed-dotted curves. For CO₂, the chemical-relaxation calculations without considering the coupling to CO and H₂O are shown in dashed-dotted curves for comparison.

APPENDIX

A. FULL EXPRESSIONS FOR THE CHEMICAL TIMESCALES

[X] represents the number density of species X in chemical equilibrium and M refers to any third body.

For $C/O \leq 1$:

$$\begin{cases} \tau_{\text{CH}_4} = \frac{[\text{CH}_4]}{k_1[\text{CH}_3][\text{OH}][\text{M}] + \max(\min(k_2[\text{CH}_2\text{OH}][\text{H}], k_3[\text{CH}_2\text{OH}][\text{M}]), k_4[\text{CH}_3][\text{O}] + k_9[\text{CH}_3\text{OH}][\text{H}] + \min(k_5[\text{C}][\text{OH}], k_6[\text{CH}_4][\text{H}]))} + \tau_{\text{H}_2} \times \frac{3[\text{CO}]}{[\text{H}_2]} \\ \tau_{\text{H}_2} = \frac{[\text{H}_2]}{k_{\text{H}}[\text{H}][\text{H}][\text{M}]} \end{cases} \quad (\text{A1})$$

$$\tau_{\text{CO}} = \frac{[\text{CO}]}{k_1[\text{CH}_3][\text{OH}][\text{M}] + \max(\min(k_2[\text{CH}_2\text{OH}][\text{H}], k_3[\text{CH}_2\text{OH}][\text{M}]), k_4[\text{CH}_3][\text{O}] + k_9[\text{CH}_3\text{OH}][\text{H}] + \min(k_5[\text{C}][\text{OH}], k_6[\text{CH}_4][\text{H}]))} + \tau_{\text{H}_2} \times \frac{3[\text{CO}]}{[\text{H}_2]} \quad (\text{A2})$$

$$\tau_{\text{H}_2\text{O}} = \frac{[\text{H}_2\text{O}]}{k_1[\text{CH}_3][\text{OH}][\text{M}] + \max(\min(k_2[\text{CH}_2\text{OH}][\text{H}], k_3[\text{CH}_2\text{OH}][\text{M}]), k_4[\text{CH}_3][\text{O}] + k_9[\text{CH}_3\text{OH}][\text{H}] + \min(k_5[\text{C}][\text{OH}], k_6[\text{CH}_4][\text{H}]))} + \tau_{\text{H}_2} \times \frac{3[\text{CO}]}{[\text{H}_2]} \quad (\text{A3})$$

For $C/O > 1$:

$$\tau_{\text{CH}_4} = \frac{[\text{CH}_4]}{k_1[\text{CH}_3][\text{OH}][\text{M}] + \min(k_2[\text{CH}_2\text{OH}][\text{H}], k_3[\text{CH}_2\text{OH}][\text{M}]) + k_9[\text{CH}_3\text{OH}][\text{H}] + \max(k_8[\text{C}_2\text{H}_2][\text{O}], k_{10}[\text{C}_2\text{H}_2][\text{OH}])} \quad (\text{A4})$$

$$\tau_{\text{CO}} = \frac{[\text{CO}]}{k_1[\text{CH}_3][\text{OH}][\text{M}] + \min(k_2[\text{CH}_2\text{OH}][\text{H}], k_3[\text{CH}_2\text{OH}][\text{M}]) + k_9[\text{CH}_3\text{OH}][\text{H}] + \max(k_8[\text{C}_2\text{H}_2][\text{O}], k_{10}[\text{C}_2\text{H}_2][\text{OH}])} \quad (\text{A5})$$

$$\tau_{\text{H}_2\text{O}} = \frac{[\text{H}_2\text{O}]}{k_1[\text{CH}_3][\text{OH}][\text{M}] + \min(k_2[\text{CH}_2\text{OH}][\text{H}], k_3[\text{CH}_2\text{OH}][\text{M}]) + k_9[\text{CH}_3\text{OH}][\text{H}] + \max(k_8[\text{C}_2\text{H}_2][\text{O}], k_{10}[\text{C}_2\text{H}_2][\text{OH}])} \quad (\text{A6})$$

$$[\text{CO}_2]_{\text{pseudo-eq}} = \frac{[\text{CO}][\text{H}_2\text{O}][\text{H}]_{\text{eq}}}{[\text{CO}]_{\text{eq}}[\text{H}_2\text{O}]_{\text{eq}}[\text{H}]} \quad (\text{A7})$$

$$\tau_{\text{CO}_2} = \frac{[\text{CO}_2]}{k_{\text{CO}_2}[\text{CO}][\text{OH}]}$$

$$\tau_{\text{NH}_3} = \frac{1}{2} \left(\frac{[\text{NH}_3]}{\max(k_{11}[\text{NH}_2][\text{NH}_2], k_{12}[\text{N}_2\text{H}_3][\text{M}]) + k_{13}[\text{NH}][\text{NH}_2] + k_{14}[\text{NO}][\text{NH}_2] + k_{15}[\text{N}][\text{NO}]} + \tau_{\text{H}_2} \times \frac{3[\text{N}_2]}{[\text{H}_2]} \right) \quad (\text{A8})$$

$$\tau_{\text{N}_2} = \frac{[\text{N}_2]}{\max(k_{11}[\text{NH}_2][\text{NH}_2], k_{12}[\text{N}_2\text{H}_3][\text{M}]) + k_{13}[\text{NH}][\text{NH}_2] + k_{14}[\text{NO}][\text{NH}_2] + k_{15}[\text{N}][\text{NO}]} + \tau_{\text{H}_2} \times \frac{3[\text{N}_2]}{[\text{H}_2]} \quad (\text{A9})$$

B. CHEMICAL PATHWAY ANALYSIS

Finding the chemical pathway is similar to the path finding problem in graph theory. That is, all species in the network are presented by nodes and reactions between them form the edges, weighted by the reaction rates (faster reactions form shorter connections). It is equivalent to finding the least time-consuming route from a starting node to an end node in the network and the total time-cost of the route can be approximated by the slowest edge (the rate-limiting step). While there are several different algorithms, e.g., [Lehmann \(2002\)](#) identifies the dominant pathways that are most efficient in removing/producing a species of interest from kinetics results with temporal evolution. We are particularly interested in finding the pathway in chemical equilibrium, which fulfills the need for estimating the chemical timescales using equilibrium abundances. For this purpose, We implement Dijkstra’s algorithm ([Dijkstra 1959](#)), which is easy to implement and highly efficient in finding fastest paths in the network problems ([Viswanath et al. 2013](#)).

Examples of comparing different chemical networks by identifying the pathways with associated rate-limiting steps are shown in Figures 7 and B3.

Below are the steps used in Dijkstra’s algorithm to find the shortest path.

1. Create a list of visited nodes (initially empty). Assign tentative distance values to all nodes: set it to zero for the initial node and to infinity for all other nodes. Set the initial node as the current node.
2. From the current node, consider all of its neighbors and calculate their tentative distances. Update the distance if the new value is smaller than the previously assigned value.
3. Include the current node in the visited-node list. A visited node will never be checked again.
4. Stop if the destination node has been marked visited. The pathway has been found and the longest edge (the slowest step) in the path is the rate-limiting step. Otherwise, select the unvisited node with the smallest tentative distance, set it as the new “current node”, and go back to step 2.

We demonstrate the steps in the following example:

Consider the simple network with nodes a-f in Figure B1. We will try to find the shortest path between a and f.

- The tentative distance values are assigned to a,b,c,d,e,f as [0, inf, inf, inf, inf, inf]. The current node is a.
- The adjacent nodes are b, d, and e. The distance values are updated to [0, 2, inf, 1, 6, inf].
- The list of visited nodes is now updated to [a]. d as the unvisited node with the smallest distance value becomes the current node.
- The adjacent nodes are c and e. The distance values are updated to [0, 2, 10, 1, 6, inf].
- The list of visited nodes is now updated to [a, d]. b as the unvisited node with the smallest distance value becomes the current node.
- We repeat the above steps (second to fifth steps in the algorithm) until f has been included in the list of visited nodes. We then have the distance values as [0, 2, 5, 1, 6, 9]. The shortest path is obtained by going back from f and following the smallest distance value. The path is a → b → c → f.

REFERENCES

- ⁸ <http://garfield.chem.elte.hu/Burcat/burcat.html>
- ⁹ Shown by Squib in the NIST database
- Agúndez, M., Venot, O., Iro, N., Selsis, F., Hersant, F., Hébrard, E., & Dobrijevic, M. 2012, A&A, 548 A73
- Agúndez, M., Parmentier, V., Venot, O., Hersant, F., & Selsis, F. 2014, A&A, 564, A73
- Bézar, B., Lellouch, E., Strobel, D., Maillard, J. P., & Drossart, P. 2002, Icarus, 159, 95

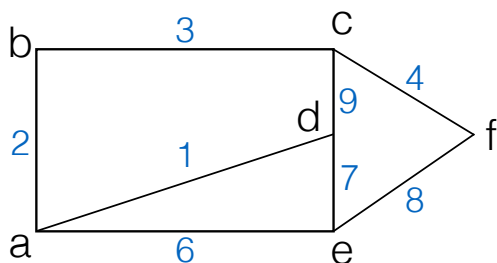


Figure B1. Finding the shortest path from a to f using Dijkstra's algorithm. There are six nodes labeled a to f connected by the edges labeled with distance. With the application to chemical networks, the nodes represent species and the edges are reactions with different rates.

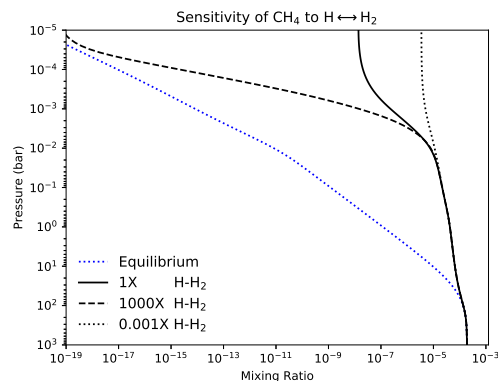


Figure B2. A sensitivity test showing how the quenching of CH_4 changes when we artificially increases/decrease the rate of $\text{H}-\text{H}_2$ dissociation/recombination by 1000 times.

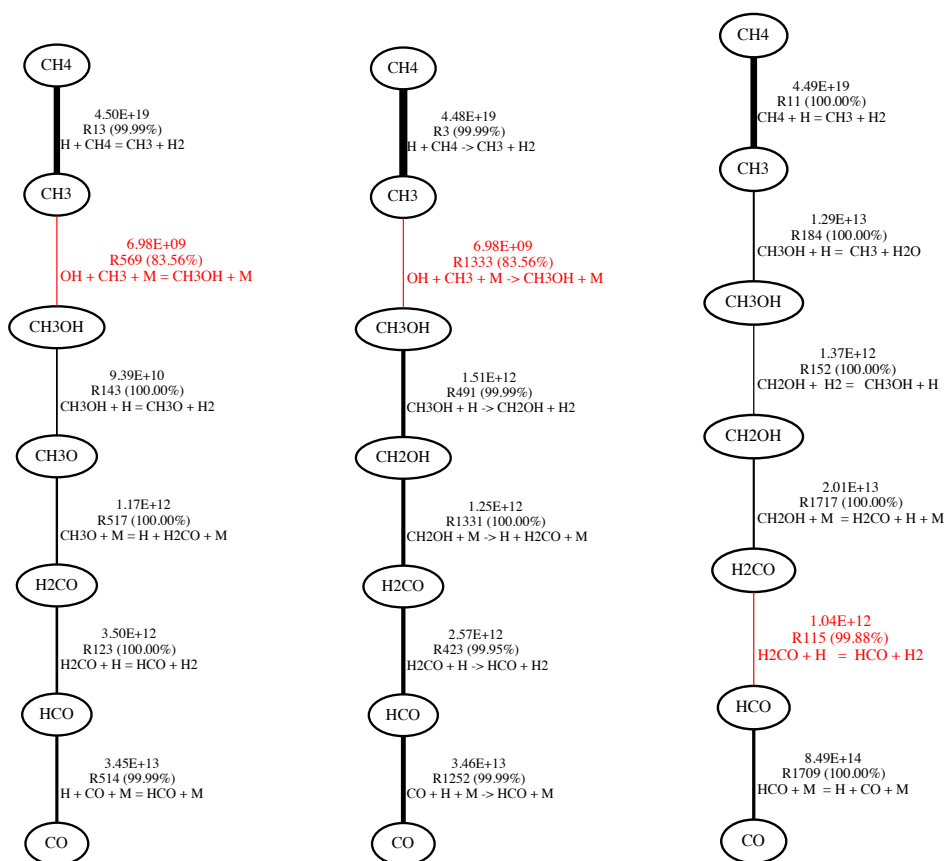


Figure B3. More examples of CH_4 -CO pathway analysis at $T = 1200$ K and $P = 500$ bar with the chemical network from VULCAN (left), Moses et al. (2011) (middle), and Venot et al. (2012) (right). Thicker lines represent faster reaction rates (denoted by the first-row numbers shown in in $\text{cm}^{-3}\text{s}^{-1}$ and the percentage of contribution to the interconversion rate is also provided) and the red lines are the rate-limiting steps. The selected temperature and pressure values are based on the CO quenched level in the deep atmosphere of Jupiter to identify the different chemical pathways as pointed out in Figure 17 of Wang et al. (2016).

Table B1. Rate-limiting reactions/steps and their rate coefficients. k_0 and k_∞ are the low-pressure and high-pressure limiting rate coefficients, respectively. The rate coefficient for the termolecular or thermal dissociation reaction is expressed by equation (28) in Tsai et al. (2017). Rev indicates the reverse reactions of Rx, which are used to derive the rate constants of Rx using the equilibrium constant calculated by the NASA polynomials⁸, as described in Appendix E in Tsai et al. (2017).

Index	Reaction	Rate Coefficient	Reference
R1	$\text{OH} + \text{CH}_3 \xrightarrow{\text{M}} \text{CH}_3\text{OH}$	$k_0 = 1.93 \times 10^3 T^{-9.88} \exp(-7544/T) +$ $5.11 \times 10^{-11} T^{-6.25} \exp(-1433/T)$ $k_\infty = 1.03 \times 10^{-10} T^{-0.018} \exp(16.74/T)$	Moses et al. (2011)
R2 _{rev}	$\text{CH}_2\text{OH} + \text{H} \longrightarrow \text{OH} + \text{CH}_3$	1.60×10^{-10}	NIST ⁹ 1987TSA471
R3	$\text{CH}_2\text{OH} \xrightarrow{\text{M}} \text{H} + \text{H}_2\text{CO}$	$k_0 = 1.66 \times 10^{-10} \exp(-12630/T)$ $k_\infty = 3 \times 10^9 \exp(-14600/T)$	NIST 1987TSA471 NIST 1975BOW343
R4	$\text{CH}_3 + \text{O} \longrightarrow \text{H}_2\text{CO} + \text{H}$	1.4×10^{-10}	NIST 1992BAU/COB411-429
R5	$\text{OH} + \text{C} \longrightarrow \text{CO} + \text{H}$	$1.05 \times 10^{-12} T^{0.5}$	NSRDS 67
R6	$\text{H} + \text{CH}_4 \longrightarrow \text{CH}_3 + \text{H}_2$	$2.20 \times 10^{-20} T^3 \exp(-4040/T)$	NIST 1992BAU/COB411-429
R7	$\text{CH}_3\text{OH} + \text{H} \longrightarrow \text{CH}_3\text{O} + \text{H}_2$	$6.82 \times 10^{-20} T^{2.685} \exp(-4643/T)$	NIST 1984WAR197C
R8	$\text{C}_2\text{H}_2 + \text{O} \longrightarrow \text{CH}_2 + \text{CO}$	$6.78 \times 10^{-16} T^{1.5} \exp(-854/T)$	NIST 1987CVE261
R9 _{rev}	$\text{CH}_3\text{OH} + \text{H} \longrightarrow \text{CH}_3 + \text{H}_2\text{O}$	$4.91 \times 10^{-19} T^{2.485} \exp(-10380/T)$	Moses et al. (2011)
R10	$\text{C}_2\text{H}_2 + \text{OH} \longrightarrow \text{CH}_3 + \text{CO}$	$8.04 \times 10^{-28} T^4 \exp(1010/T)$	NIST 1989MIL/MEL1031-1039
R11	$\text{NH}_2 + \text{NH}_2 \longrightarrow \text{N}_2\text{H}_2 + \text{H}_2$	$2.89 \times 10^{-16} T^{1.02} \exp(-5930/T)$	NIST 2009KLI/HAR10241-10259
R12	$\text{N}_2\text{H}_3 + \xrightarrow{\text{M}} \text{N}_2\text{H}_2 + \text{H}$	$k_0 = 3.49 \times 10^{38} T^{-13.13} \exp(-36825/T)$ $k_\infty = 7.95 \times 10^{13} \exp(-27463/T)$	Hwang & Mebel (2003)
R13	$\text{NH} + \text{NH}_2 \longrightarrow \text{N}_2\text{H}_2 + \text{H}$	$6.98 \times 10^{-10} T^{-0.27} \exp(39/T)$	NIST 2009KLI/HAR10241-10259
R14	$\text{NO} + \text{NH}_2 \longrightarrow \text{N}_2 + \text{H}_2\text{O}$	$7.9 \times 10^{-9} T^{-1.1} \exp(-98/T)$	NIST 1994DIA/YU4034-4042
R15	$\text{N} + \text{NO} \longrightarrow \text{N}_2 + \text{O}$	3.7×10^{-11}	NIST 1992MIC/LIM3228-3234
R16	$\text{N}_2\text{H}_4 + \text{H} \longrightarrow \text{N}_2\text{H}_3 + \text{H}_2$	$1.17 \times 10^{-11} \exp(-1260/T)$	NIST 1995VAG777-790
k_{H}	$\text{H} + \text{H} \xrightarrow{\text{M}} \text{H}_2$	$k_0 = 2.7 \times 10^{-31} T^{-0.6}$ $k_\infty = 3.31 \times 10^{-6} T^{-1}$	NIST 1992BAU/COB411-429 NIST 1965JAC/GIE3688
k_{CO_2}	$\text{CO} + \text{OH} \longrightarrow \text{CO}_2 + \text{H}$	$1.05 \times 10^{-17} T^{1.5} \exp(259/T)$	NIST 1992BAU/COB411-429

- Burrows, A., & Sharp, C.M. 1999, *ApJ*, 512, 843
- Cooper, C. S., & Showman, A. P. 2006, *ApJ*, 649, 1048
- Cribb, P. H., Dove J. E., Yamazaki S. A. 1992 *Combust Flame*, 88, 169
- Dean, A. M., & Bozzelli, J. W. 2000, in *Gas Phase Combustion Chemistry*, ed. W. C. Gardiner, Jr. (New York: Springer), 125
- Dijkstra, E. W. 1959 *Numer. Math.* 1, 269
- Dobbs-Dixon, I., & Agol, E. 2013, *MNRAS*, 435, 3159 (DA)
- Drummond, B., Mayne, N. J., Manners, J., et al. 2018, *ApJL*, 855, 2, L31
- Grassi, T., Bovino, S., Schleicher, D. R. G., J. Prieto, D. Seifried, E. Simoncini, F. A. Gianturco 2014, *MNRAS*, 439, 2386
- Greenhill, P. G., O'Grady, B. V., Gilbert, R. G., 1986, *Aust. J. Chem.*, 39, 1929
- Griffith, C. A., & Yelle, R. V. 1999, *ApJ*, 519, L85
- Held, I.M., & Suarez, M.J. 1994, *Bulletin of the American Meteorological Society*, 75, 1825
- Held, I.M. 2005, *Bulletin of the American Meteorological Society*, 86, 1609
- Heng, K., Mendonça, J.M., & Lee, J.-M. 2014, *ApJS*, 215, 4
- Heng, K., & Showman, A.P. 2015, *Annual Review of Earth and Planetary Sciences*, 43, 509
- Heng, K., & Tsai, S.-M. 2016, *ApJ*, 829, 104
- Hidaka, Y., Oki, T., Kawano, H. 1989, *J. Phys. Chem.* 93 (20), 7134
- Hu, R., Seager, S., & Bains, W. 2012, *ApJ*, 761, 166
- Hu, R., & Seager, S. 2014, *ApJ*, 784, 63
- Hunter, J. D. 2007, *Computing In Science & Engineering*, 9, 90
- Hwang, D.-Y., Mebel, A.M. 2003, *J. Phys. Chem. A*, 107, 2865
- Jasper, A., Klippenstein, S. J., Harding, L. B., & Ruscic, B., 2007, *J. Phys. Chem. A*, 111, 3932
- Lehmann, R., 2002, *J. Atmos. Chem.* 41, 297
- Kopparapu, R.K., Kasting, J.F., & Zahnle, K.J. 2012, *ApJ*, 745, 77
- Lodders, K., & Fegley, B., Jr. 2002, *Icarus*, 155, 393
- Lodders, K. 2009, in *Formation and Evolution of Exoplanets*, ed. R. Barnes (Berlin: Wiley), 157
- Line, M. R., Liang, M. C., & Yung, Y. L. 2010, *ApJ*, 717, 496 1004.4029
- Madhusudhan, N., & Seager, S. 2011, *ApJ*, 729, 41
- Madhusudhan, N. 2012, *ApJ*, 758, 36
- Mendonça, J.M., Grimm, S.L., Grosheintz, L., & Heng, K. 2016, *ApJ*, 829, 115
- Moses, J. I., Visscher, C., Fortney, J., et al. 2011, *ApJ*, 737, 15
- Moses, J.I., Madhusudhan, N., Visscher, C., & Freedman, R. 2013a, *ApJ*, 763, 25
- Moses, J.I., et al. 2013b, *ApJ*, 777, 34
- Moses, J.I. 2014, *Phil. Trans. Roy. Soc. A* 372
- Moses, J. I., Marley, M. S., Zahnle, K., et al. 2016, *ApJ*, 829, 66
- Page, M., Lin, M. C., He, Y., & Choudhury, T. 1989, *J. Phys. Chem.*, 93, 4404
- Prinn, R.G., & Barshay, S.S. 1977, *Science*, 198, 1031
- Rimmer, P. B., & Helling, C. 2016, *ApJS*, 224, 9
- Rocchetto, M., Waldmann, I. P., Venot, O., et al. 2016, *ApJ*, 833, 120
- Showman, A. P., Fortney, J. J., Lian, Y., et al. 2009, *ApJ*, 699, 564
- Smith, M. D. 1998, *Icar*, 132, 176
- Stock J.W., Kitzmann D., Patzer A.B.C., et al. submitted (arXiv:1804.05010)
- Tsai S.-M., Lyons J. R., Grosheintz L., et al. 2017, *ApJS*, 228, 20
- Tsang, W. 1987, *J. Phys. Chem.*, 16, 471
- Turányi T. 1990, *J. Math. Chem.* 5, 203
- van der Walt, S., C., C., & Varoquaux, G. 2011, *Computing in Science & Engineering*, 13, 22
- Venot, O., Hébrard, E., Agúndez, M., Dobrijevic, M., Selsis, F., Hersant, F., Iro, N., & Bounaceur, R. 2012, *A&A*, 546, A43
- Venot, O., Hébrard, E., Agúndez, M., Decin, L., & Bounaceur, R. 2015, *A&A*, 577, A33
- Viswanath S., Kreuzer S. M., Cardenas A. E., & Elber R. 2013, *J. Chem. Phys.*, 139, 17
- Venot, O. & Agúndez, M. 2015, *Exp Astron*, 40, 469
- Visscher, C., Moses, J. I., & Saslow, S. A. 2010, *Icarus*, 209, 602
- Visscher, C., Moses, J. I., 2011, *ApJ*, 738, 72
- Visscher C., 2012, *ApJ*, 757, 5
- Wang, D., Lunine, J.I., Mousis, O. 2016, *Icarus*, 276, 21
- Yung, Y. L., Drew, W. A., Pinto, J. P., & Friedl, R. R. 1988, *Icarus*, 73, 516
- Zahnle, K. J., & Marley, M. S. 2014, *ApJ*, 797, 41